



Surface Pressure Study of an Airfoil Undergoing Combined Pitch and Low-Amplitude Plunge Motions

A. Tabrizian, M. Masdari[†] and M. Tahani

University of Tehran, Tehran, 14395 -1561, Iran

[†]Corresponding Author Email: m.masdari@ut.ac.ir

(Received November 6, 2018; accepted January 30, 2019)

ABSTRACT

This paper describes the experimental study of surface pressure over a supercritical airfoil which was oscillated in pure pitching, pure plunging and combined pitch-plunge motions at the Reynolds number of 8.76×10^5 . While the surface pressure distribution is of significant importance in stability and performance of an airfoil, not sufficient information is available on the pressure distribution in dynamic stall. The experiments were conducted in a closed-loop wind tunnel utilizing pressure transducers array. The motions were designed to maintain constant reduced frequency, Strouhal number and phase difference. Three different regions were assumed to represent the pressure distribution over the airfoil. The results showed that LEV formed on the upper surface manifested different behavior. In the attached flow region the LEV grew and shrunk over the upper surface but in the light stall region the LEV spilled on the airfoil while a small partial LEV remained at the leading edge. In the deep stall region the LEV spilled entirely and the flow was fully separated. The formation of Laminar Separation Bubbles and suction peaks were also reported in low angles of attack. Besides, the pitching moment Damping Factor was studied to determine the level of airfoil stall flutter stability. For lower amplitudes of pitching motion the airfoil seemed to be stable except where deep stall occurred. However for high amplitudes the airfoil had a tendency to enter the stall flutter. Nevertheless, forcing the airfoil to undergo a combined motion improved the stability condition in all cases.

Keywords: Combined pitch-plunge motion; Dynamic stall; Experimental unsteady aerodynamics; Supercritical airfoil.

NOMENCLATURE

c	chord length	St	Strouhal number ($f h_0 / U_\infty$)
C_p	pressure coefficient	T	cycle period
C_l	lift force coefficient	U_∞	freestream velocity
C_m	pitching moment coefficient	α_0	mean AOA
DSV	Dynamic Stall Vortex	α_{eff}	angle of attack (AOA)
f	frequency of motion	α_{pitch}	pitch AOA
h	plunge position	α_{plunge}	plunge AOA
h_0	plunge amplitude	ζ	damping factor (DF)
k	reduced frequency ($\pi f c / U_\infty$)	θ_0	pitch amplitude
LEV	Leading Edge Vortex	φ	phase difference between h and α_{pitch}
LSB	Laminar Separation Bubble	ω	angular velocity

1. INTRODUCTION

Nowadays, unsteady aerodynamics is one of the most interesting subjects, drawing the attention of large population of researchers. The focus on dynamic stall is remarkably increasing. Rising popularity of MAVs, simulation and comprehensive understanding the insect's flight, thrust production

from moving airfoils, flight performance improvement and many other novel phenomena are results of studying of unsteady aerodynamics. Also, investigating the time varying aerodynamic forces is very common to give an insight of aeroelasticity and fluid-structure interaction problems. The nonlinear behavior of forces and moments during dynamic stall introduces the aeroelasticity instabilities such as stall

flutter. Furthermore, examination of different types of motions is a common way to extract some dynamic stability coefficients of an aircraft. Hence, some complicated stability derivatives and their contribution on the airfoil can be achieved by exciting the airfoil with forced combined motions.

At the beginning of the unsteady aerodynamics, Theodorsen *et al.* (1935) calculated forces and moments over an airfoil undergoing a pure pitching motion. The theoretical results showed that under the condition of no separation, a hysteresis exists in the values of forces and moments. He explained that the interaction of circulatory and apparent mass part of the forces will result in a lag or lead in flow. McCroskey (1982) published a thorough study on different features and regions of dynamic stall over a NACA0012 airfoil. His work followed by McAlister *et al.* (1978); He conducted a series of experimental investigations on the dynamic stall of an airfoil under various conditions of tests. Carr and Cebeci (1985) studied the influence of transition location on boundary layer separation. They noticed that in upstroke motion, the location of transition moves toward the upstream and totally dependent on the motion frequency. Experimental and computational analyses of Radespiel *et al.* (2007) demonstrated the important role of transition and turbulence in the unsteady aerodynamic of flapping airfoils at Reynold's numbers ranges equaling those of birds and MAVs. Meanwhile, many other experimental and numerical investigations were performed and shed some light to the complicated aspects of dynamic stall in pitching and plunging oscillations (Gerontakos, 2004; Jones and Platzer, 1998; Koochesfahani, 1989; Lian *et al.*, 2008; Masdari *et al.*, 2017; Mulleners and Raffel, 2012; Raffel *et al.*, 1995; Lai and Platzer, 1999; Sarkar and Venkatraman, 2008; Young and Lai, 2004).

More recent, Gharali and Johnson (2014) reported an examination on the dynamic stall of an oscillating airfoil for a range of reduced frequencies. They calculated aerodynamic loads based on the control-volume approach by post-processing of fast-response particle image velocimetry (PIV) data. Also, (Negi *et al.*, 2017; 2018) used LES approach to investigate the transition phase of flow around an airfoil in small amplitude pitch motion. Masdari *et al.* (2018) represented a new approach for a better understanding of lift hysteresis. They used a new parameter, Normal Force Defect (NFD), which correlates with the value of lead or lag in flow field during any oscillatory motion.

In recent years, some researchers have intended to examine the combined unsteady motions such as pitch-hold and return and concurrent pitching and plunging motions.

Freytmuth (1990), conducted an experiment on a hovering flat plate in combined pitch-plunge motion. He noticed that the Von-Karman vortices have a great impact in thrust production of the flat plate. Isogai *et al.* (1999) studied the effects of dynamic stall on propulsive efficiency and generated thrust over an airfoil undergoing simultaneous pitching and plunging motion with a computational approach. They concluded that the highest value of propulsive

efficiency is achieved when the pitching motion has a 90 degrees phase lag with regard to plunging motion. Moreover, preventing the formation of leading edge vortices aids to attain highest value of propulsive efficiency as reported by Tuncer and Kaya (2003).

McGowan *et al.* (2009) presented a study on an airfoil experiencing pure pitching and plunging motions in the Reynold's number of 10^4 utilizing analytical, numerical and experimental solutions. They showed that for low amplitudes motions with a specific phase difference, the value of lift generated by pitching motion, could be canceled by plunging motion. In other words, for a pitching airfoil with low amplitudes, there is an equivalent plunging motion. This will lead to achieving a unique lift force that is equal to the steady state lift force. Rival and Tropea (2010) performed a set of experiments on the dynamic stall of a SD7003 pitching, plunging and combined motions airfoil and found that with increasing the reduced frequency and lag of the shed vortices, the direction of lift hysteresis is reversed. Baik *et al.* (2009) carried out an experimental comparison between SD7003 and flat plate model undergoing pitching and plunging motion. The flow topology and wall velocity profiles from the PIV measurements showed a Reynolds dependent behavior for SD7003 where the extent of flow separation is reduced at a relatively high Reynolds. On the contrary, flat plate displayed a large leading edge separation and flow characteristics that were independent of Reynolds. It was also proven that the difference in the leading edge shape caused delayed formation and development of LEV during the downstroke motion. In another survey done by Baik *et al.* (2010) the formation of a leading and trailing edge vortices was considered. It is revealed that the formation phase of the LEV is dependent on the reduced frequency.

In a similar research, Kang *et al.* (2009) performed both experimental and computational studies in order to examine the effects of Reynolds number on the SD7003 airfoil during pitching and plunging motion and an excellent agreement was reported when no separation occurred. Besides, computed lift coefficient time history was compared with Theodorsen's unsteady linear airfoil theory which indicated acceptable agreement when the flow was attached.

In this paper the surface pressure distribution of an airfoil undergoing pure pitching, pure plunging and combined pitching and plunging motions with fixed phase difference is studied experimentally. The aim of this work is to present an insight into the physics of dynamic stall on a specific supercritical airfoil and its consequences by focusing on pressure distribution. Many recent works, as mentioned earlier, considered the dynamic stall problem using direct force measurement and flow visualization. However, published data on pressure distribution are scarce. Besides, almost all studies are carried out on conventional airfoils and less information can be found on supercritical airfoils. Since any aircraft experiences low speeds during takeoff and landing phases of flight, it is desired to investigate the airfoil

dynamic stall behavior in low subsonic regime. Also, some valuable information, gathered from pressure distribution such as the flow separations, reattachments and formed vortices on the surface is presented in the current paper. Furthermore, since the aeroelastic stability of an airfoil during unsteady motion is a very important issue nowadays, a brief discussion is provided on the airfoil's stability during above maneuvers using a quantitative parameter, termed as Damping Factor.

2. EXPERIMENTAL APPARATUS

The tests were conducted in a Göttingen-type, open test section wind tunnel with test section dimensions of 2.4 m*2.8 m. A 1.6 MW AC induction motor along with a 9:1 contraction ratio assures the maximum velocity of 60 m/s in the test section at the standard room temperature. The settling chamber of the wind tunnel is equipped with a honeycomb and two screens in order to maintain the turbulence intensity below 0.35%. To reduce the effects of open test section jet flow and to ensure the acceptable margins of uniformity of the flow over the model, a 2.5 m*1 m wooden test section was employed. A stainless steel supercritical infinite airfoil section with chord length of 40 cm and maximum thickness of 9.8% was placed just after the contraction where the turbulence intensity measured by hotwire was approximately 0.3% at 35 m/s. 66 and 67 pressure tabs on upper and lower surfaces were embedded to measure on-surface pressure. In order to guarantee the 2D flow and roll-up prevention of tip vortices, two wooden circular plates, each 1 m in diameter, were positioned at the both ends of the airfoil. The airfoil pure pitch and plunge motions were generated by two separate four-bar linkage mechanisms in conjunction with two servo motors, controlled by a LabVIEW™ based program. For the combined pitch and plunge motion, however, the pitching system was used as the generator of both motions. The output rotation of the servo motor is translated to the pitching system similar to pure pitching system. To produce the plunge motion, plunging system is connected to the same motion of pitching via a mechanical link, connected to a fixed part of the mechanism. This could assure that the frequency of both motions were exactly the same during the test. Also four sets of springs were designed to reduce the impact of plunge motion without any effect on sinusoidal trajectory of the wing.

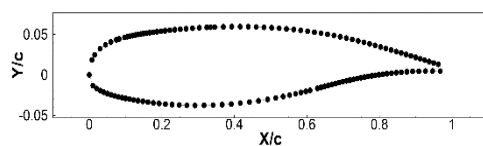


Fig. 1. Airfoil geometry and pressure tabs arrangement.

The surface pressure was measured by a set of 10 mbar and 60 mbar self-amplified high accuracy piezoelectric transducers that were connected to the pressure tabs via plastic tubes. The accuracy of the sensors is 0.5% FSO and the corresponding time lag

of the tubes was measured about 0.005 s which enabled us to acquire data at the rate of 200 Hz. Three independent 16-bit A/D devices were synchronized by an external analogue signal and were employed to collect the transducers output. All operations were controlled through a LabVIEW™ code.

A process of uncertainty calculation was carried out at the confidence level of 95% and the maximum uncertainty of lift coefficient comprising both bias and precision errors was obtained about 2.5%.

With the purpose of recording the angle of attack in pitch motion a digital shaft encoder was directly connected to the airfoil rotation axis at c/4. Equation (1) shows the relation of angle of attack with time. Also an analogue potentiometer was used to determine the translation of the airfoil during the plunge motion. This motion is defined in Eq. (2).

$$\theta(t) = \alpha_0 + \theta_0 \sin(\omega t + \varphi) \quad (1)$$

$$h(t) = h_0 \sin(\omega t) \quad (2)$$

Where θ is geometric angle of attack, α_0 is the mean angle of attack, θ_0 represents the pitching amplitude, ω is angular velocity, φ is phase difference between pitching and plunging motion, h_0 is plunge amplitude and h is translation of the airfoil during plunge motion.

Hence, the effective angle of attack in the combined pitching and plunging motion can be calculated as below:

$$\alpha_{\text{eff}} = \alpha_{\text{pitch}} + \alpha_{\text{plunge}} \quad (3)$$

$$\alpha_{\text{eff}} = \alpha_0 + \theta_0 \sin(\omega t + \varphi) - \text{Arctg}\left(\frac{\dot{h}}{V}\right) \quad (4)$$

Making some modification and simplification to Eq. (4) and neglecting the non-linearity of inverse tangent for small angles, it can be re-written as below.

$$\alpha_{\text{eff}} = \alpha_0 + \theta_0 \sin(2\pi f t + \varphi) - 2\pi \text{St} U_\infty \cos(2\pi f t) \quad (5)$$

Where, St is the Strouhal number and f is physical frequency of motion.

It is worth noticing that in this study, the phase difference between effective angles of attack in combined motion is 90 degrees as shown Fig. 2.

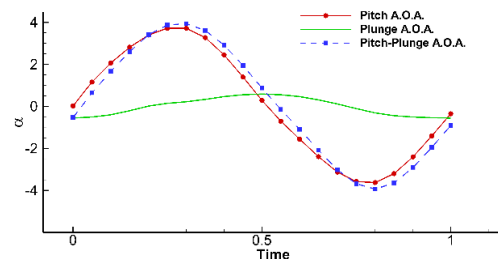


Fig. 2. Sample of pitching, plunging and effective angle of attack.

Table 1 Test plan

	α_0	θ_0	Pure Pitch		Pure Plunge		Pitch-Plunge	
			α_{min}	α_{max}	α_{min}	α_{max}	α_{min}	α_{max}
Attached flow	0	4	-4	4	-0.61	0.61	-4.04	4.04
	0	12	-12	12	-0.61	0.61	-12.01	12.01
	8	4	4	12	-0.61	0.61	3.96	12.01
Light Stall	8	12	-4	20	-0.61	0.61	-4.01	20.01
	14	4	10	18	-0.61	0.61	9.96	18.04
Deep Stall	14	12	2	26	-0.61	0.61	1.99	26.01

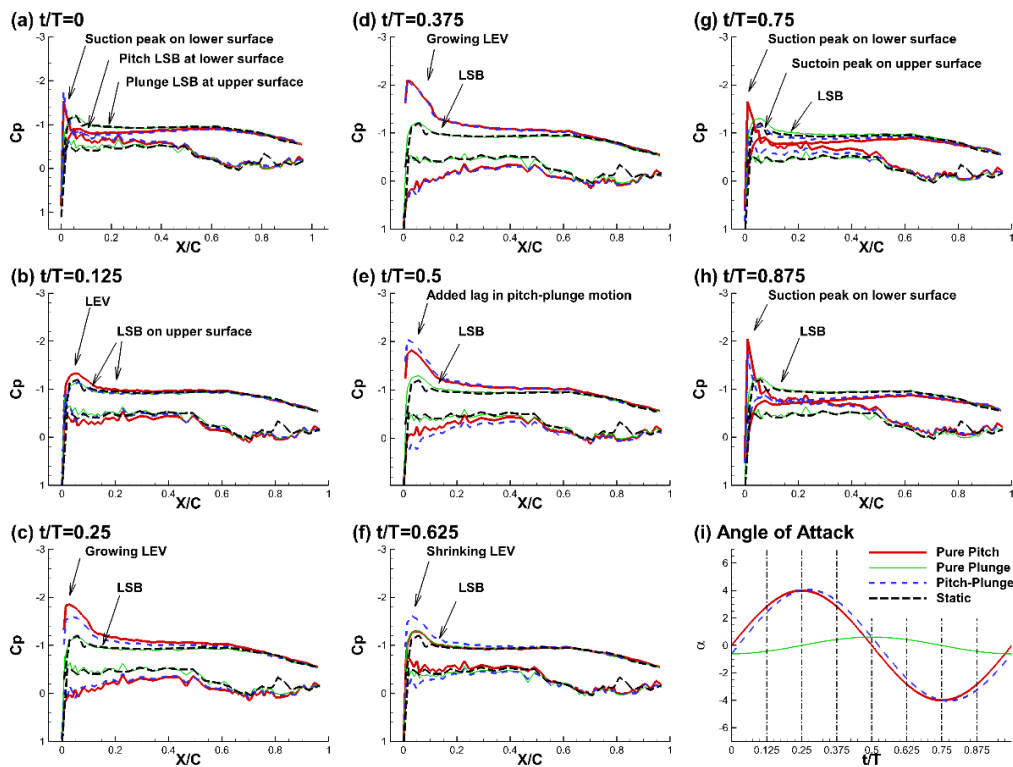


Fig. 3. Coefficient of pressure distribution for $\alpha_0=0$, $\theta_0=4$ and $h_0=60$ mm in different time intervals as shown on figures (a) to (h) and (i) is the angle of attack. Thick red solid line is pure pitching, normal green line is pure plunging and dashed blue line is combined pitch-plunge motion

3. RESULTS AND DISCUSSION

The surface pressures and consequent coefficients of lift and pitching moments over a supercritical airfoil are investigated in this paper. The results are classified in a way to enable one to study and compare three regions of attached flow, light stall and deep stall over the airfoil that is subjected to pure pitching, pure plunging and combined pitching and plunging motions. In order to cover these three regions, the value of mean angle of attack and the amplitude of motion are selected as mentioned in Table 1. For the better comparison, the results are

presented at the fixed free stream velocity of 35 m/s corresponding to Reynolds number of 8.76×10^5 , plunge amplitude of 60 mm and reduced frequency of 0.035. Hence, the value of Reynolds, Strouhal number and reduced frequency are constant in this paper.

3.1 Attached flow Region

The pressure distributions over the upper and lower surfaces of the airfoil with $\alpha_0=0$ and $\theta_0=4$ are depicted in Fig. 3 for the intervals of $T/8$. At the start of the motion, Fig. 3(a), a small suction peak is observed on the lower surface, followed by a

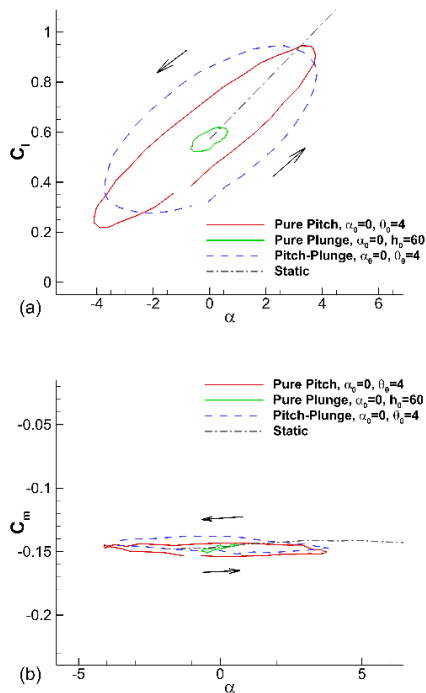


Fig. 4. (a) Lift coefficient (b) Pitching moment for $\alpha_0=0, \theta_0=4$ and $h_0=60$ mm.

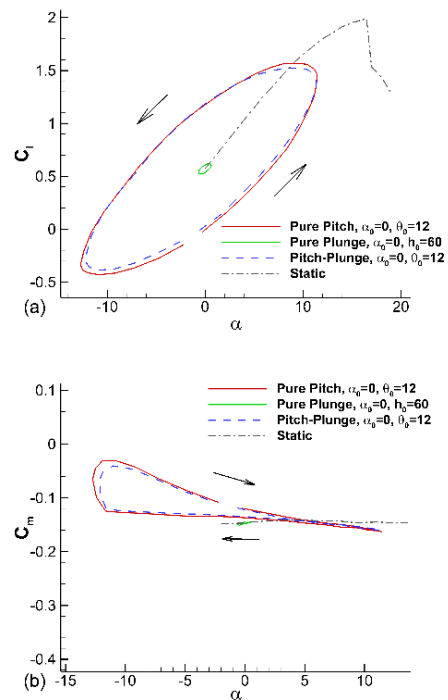


Fig. 5. (a) Lift coefficient (b) Pitching moment for $\alpha_0=0, \theta_0=12$ and $h_0=60$ mm.

Laminar Separation Bubble (LSB) during the pure pitching and combined motions. The LSB is also visible over the entire plunging motion on the upper surface. Since the plunge amplitude is small, there is no significant change detected in the coefficient of pressure during this motion for all cases and they are roughly identical. Also the effects of concave lower surface at near-trailing edge region of the airfoil are obvious. This curvature is designed to compensate the loss of lift force due to flat upper surface of the supercritical airfoils. However, a great nose-down pitching moment is generated by these airfoils. The middle flat part of pressure coefficient on upper surface can be attributed to the flat geometry of upper surface which produces a slight positive pressure gradient, accordingly causes a slight increase in pressure coefficient. At $t/T=0.125$ the lower suction peak vanishes and the flow accelerates and a short LSB is also formed over the upper surface. As the angle of attack increases a Leading Edge Vortex (LEV) appears gradually and starts to grow which leads to greater velocity and causes a stronger suction over the airfoil. Due to the lag in the boundary layer flow, the growth of the LEV continues even after the maximum angle of attack ($t/T=0.25$) and within downstroke motion as shown in Fig. 3(d). The strength of LEV decreases as the airfoil downstroke motion continues, but no evidence of the LEV spillage and vortex shedding is seen in pressure coefficients. The LEV just slightly shrinks over the upper surface and disappears with decreasing the angle of attack from $t/T=0.5$ to 0.75.

Although in this study the plunge effective angle of attack is small and the pressure coefficient is more

impressed by the pitching motion, it should be noticed that adding plunge motion will result in a slight added lag in the flow field of the combined motion. This added lag is presented in Fig. 3(g) where the LEV has still the maximum negative pressure coefficient in the combined motion, while it has started to shrink in the pure pitch motion. As the airfoil experiences more negative angles of attack (see Fig. 3(g)), the suction peak in pitching motion moves to lower surface, while during the combined motion the airfoil still carry the suction peak in its upper surface as well.

Figure 4(a) and Fig. 5(a) illustrate the lift coefficients of the airfoil for the motions about the mean angle of attack of zero with pitching amplitudes of 4 and 12. As shown in the figures a hysteresis loop in lift coefficients is produced due to the phase lag of the unsteady motion where the arrows on the figures show the loops counter clockwise direction. The wider hysteresis loop during combined pitch and plunge motion implies the greater phase lag in boundary layers of both upper and lower surfaces which is in good agreement with the pressure distribution results, called added lag. Furthermore, for the lower amplitude of motion, the lag is more remarkable because the effects of plunging motion are more noticeable at lower pitching amplitude, while for the higher pitch amplitude, the pitching motion is totally dominant and the lift coefficients in both pitch and combined pitch and plunge motions are approximately identical. Also, the value of lift coefficient is increased in higher amplitude as expected.

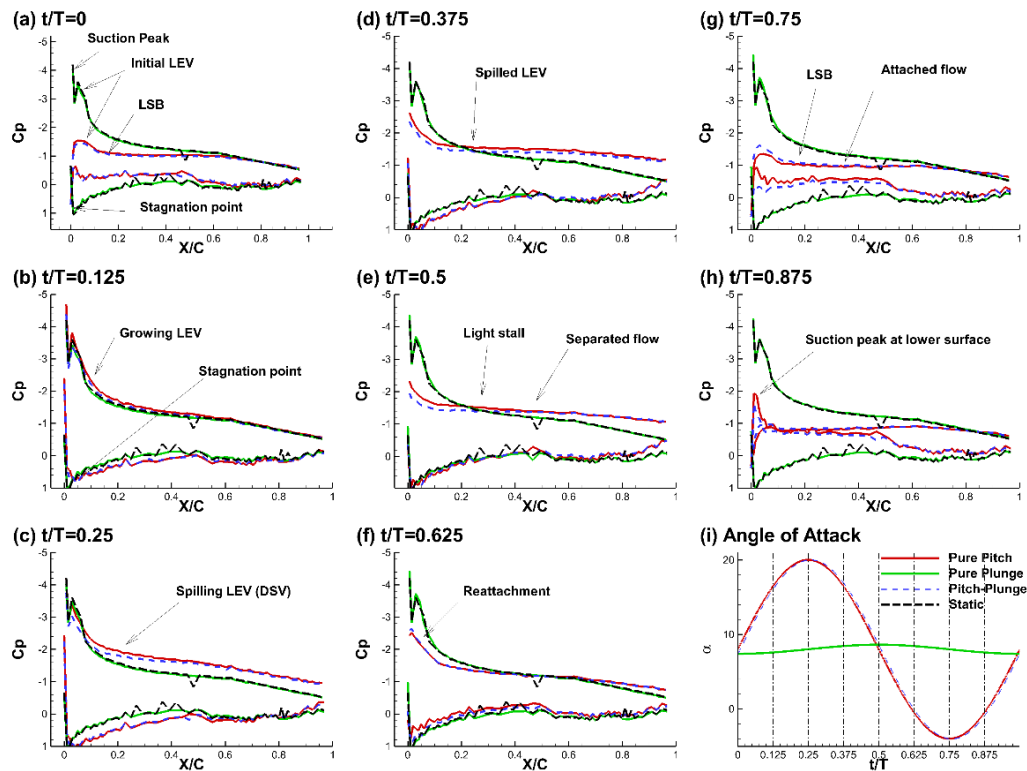


Fig. 6. Coefficient of pressure distribution for $\alpha_0=8$, $\theta_0=12$ and $h_0=60$ mm in different time intervals as shown on figures (a) to (h) and (i) is the angle of attack. Thick red solid line is pure pitching, normal green line is pure plunging and dashed blue line is combined pitch-plunge motion.

The coefficients of pitching moment for above cases are depicted in Fig. 4(b) and Fig. 5(b). The value of pitching moment for the airfoil is negative that shows the airfoil tends to nose-down condition during the flight. As no stall exists on the airfoil, the direction of pitching moment hysteresis loop is constant and counter clockwise for lower motion amplitude over the entire motion, while for higher motion amplitude the direction of pitching moment hysteresis is reversed and the airfoil encounters an instability tendency at the end of the downstroke motion, represented with a jump in positive direction in pitching moment. This positive jump can be attributed to the high negative angles of attack and the flow separation on lower surface. It can be interpreted that with increasing the amplitude of pitching in both pure and combined motion, the airfoil enters the stall flutter instability.

Additionally, this airfoil has higher values of pitching moment at low angles of attack in comparison to the conventional airfoils (Leishman, 2006). Higher phase lag in combined motion is seen, as well. The stability of the airfoil discussed in detail in the last section.

3.2 Light Stall Region

The coefficients of pressure for pure pitch, pure plunge and combined pitching and plunging motions with $\alpha_0=8$ and $\theta_0=12$ are presented in Fig. 6. At the start of the motion a small LEV is observed over the upper surface for all three motions which are accompanied by a suction peak in the plunge motion.

As discussed in previous section, no remarkable change is found in coefficient during the pure plunge motion. Also a LSB can be seen in pure pitch and combined motion. The strength of the LEV in both pure pitch and combined motion grows with increasing the angle of attack and at $t/T=0.25$ the LEV starts to spill over the upper surface. At $t/T=0.375$ the LEV sheds from the upper surface and the airfoil experiences a light stall until $t/T=0.625$. However over all duration of the stall, a marginal peak in upper surface pressure coefficient exists. Figure 6(f) shows the beginning of the flow reattachment at the upper surface where an increase in the pressure coefficient magnitude is sensed due to attached flow acceleration. In next time step the flow is fully attached, but the value of the C_p is dipped because of a decrement in the angle of attack. Finally at the negative angles of attack the suction peak moves to the lower surface as shown in Fig. 6(h). Moreover, the stagnation point at the start of the motion ($t/T=0$) was located at the leading edge, but it moves along the lower surface and towards the trailing edge as the angle of attack increases and continues a reverse motion as the angle of decreases along with a lag and after $t/T=0.625$.

Figure 7(a) displays the lift coefficient of the airfoil undergoes pure pitching, plunging and combined pitching and plunging motions about 8° angle of attack with 12° amplitude. Since the mean angle of attack is increased the slope of lift hysteresis decreased and the airfoil enters a light dynamic stall at the end of the upstroke motion.

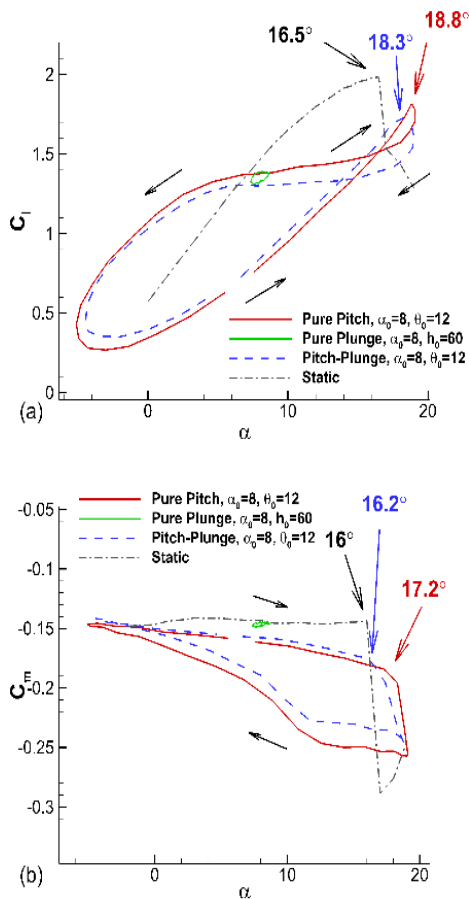


Fig. 7. (a) Lift coefficient (b) Pitching moment for $\alpha_0=8$, $\theta_0=12$ and $h_0=60$ mm.

For pure pitching motion the airfoil stalls at 18.8° and for combined motion the stall occurs at 18.3° , while the stall condition does not appear in pure plunge motion. Besides the maximum lift coefficient and the angle of attack of the cross-over point in hysteresis slightly decrease and the flow reattaches later when the airfoil undergoes the combined motion. No noticeable change in the flow lag is detected since at high amplitude motion the pitching motion is the most influential parameter on the airfoil behavior. Also the pitching moment coefficient depicted in Fig. 7(b), implies the stall condition in a smaller angle of attack as expected.

The airfoil pitching moment stalls at 17.2° in the pitching motion and 16.2° in the combined motion. This early stall can be attributed to the Dynamic Stall Vortex (DSV) spillage over the upper surface of the airfoil.

As long as the DSV exists on the upper surface the lift force is generated and the lift stall does not occur, while as the DSV is spilling toward the trailing edge, more lift force is generated from near-trailing edge side of the airfoil and thus a negative pitching moment is produced. So, the difference between lift force and pitching moment stall angles could be an evidence for DSV spillage on the upper surface of

the airfoil. Furthermore, the pitching moment hysteresis is clockwise and tends towards instability and no figure eight shape is seen in the light stall region.

3.3 Deep Stall Region

Figure 8 shows the pressure distribution in the same abovementioned motions with a higher mean angle of attack, $\alpha_0=14$, and amplitude of 12° . Unlike light stall region, no initial suction peak is detected. However a long stationary LEV is seen on the upper surface of the airfoil during plunge motion, while the smaller one is detected in pure pitching and combined motion at start of motion cycle. This LEV grows rapidly as the motion progresses until $t/T=0.1$ and before reaching to maximum angle of attack spills on the upper surface. The extent of DSV is much larger and it spills a little bit later in the pure pitching rather than the combined motion. From this time on ($t/T=0.375$), the flow is fully separated and no evidence of even tiny LEV can be observed near the leading edge in contrast with the light stall region. The reattachment process takes place sooner in the combined motion as depicted in Fig. 8(f). At $t/T=0.9$ the flow is seems to be fully attached and the process continues with formation of a small LEV close to leading edge. Despite of two previous sections, no suction peak appears on the lower surface since the angle of attack is always positive in this motion. Furthermore, the stagnation point is located on the lower surface during the whole cycle and it moves towards the trailing edge as the angle of attack increases and vice versa.

The coefficient of lift is also plotted in Fig. 9(a). The lift coefficient reaches higher values in pure pitching motion and stalls at the higher angle of attack. In other words imposing the low amplitude plunge to pitching motion enhances the stall angle from 23.8° to 20.7° and the cross over point takes place at lower angles. Also it can be seen that at the right side of cross over point lift values in both motions are clockwise and are accompanied by a phase lead, but this lead is greater as the airfoil subjected to the combined motion. This lead in the right side of the cross over point brings about an enhanced reattachment which agrees with pressure distribution results (Fig. 8(f)).

Figure 9(b) illustrates the pitching moment coefficient in deep stall region. As expected the pitching moment stall occurs in lower angles of attack regarding to lift stall. Repeatedly, the combined motion stalls at lower angles (18.9°) in comparison to pure pitch motion (21.1°). In the deep stall region a figure eight and a deeper stall occurrence are observed in pitching moment which can be explained by the missing tiny LEV at stall condition regarding the light stall region; since an LEV in near-leading edge regions is able to impose a nose up pitching moment. Besides, the cross over point in combined motion happens in lower angles of attack due the phase lead and this can result in higher stability.

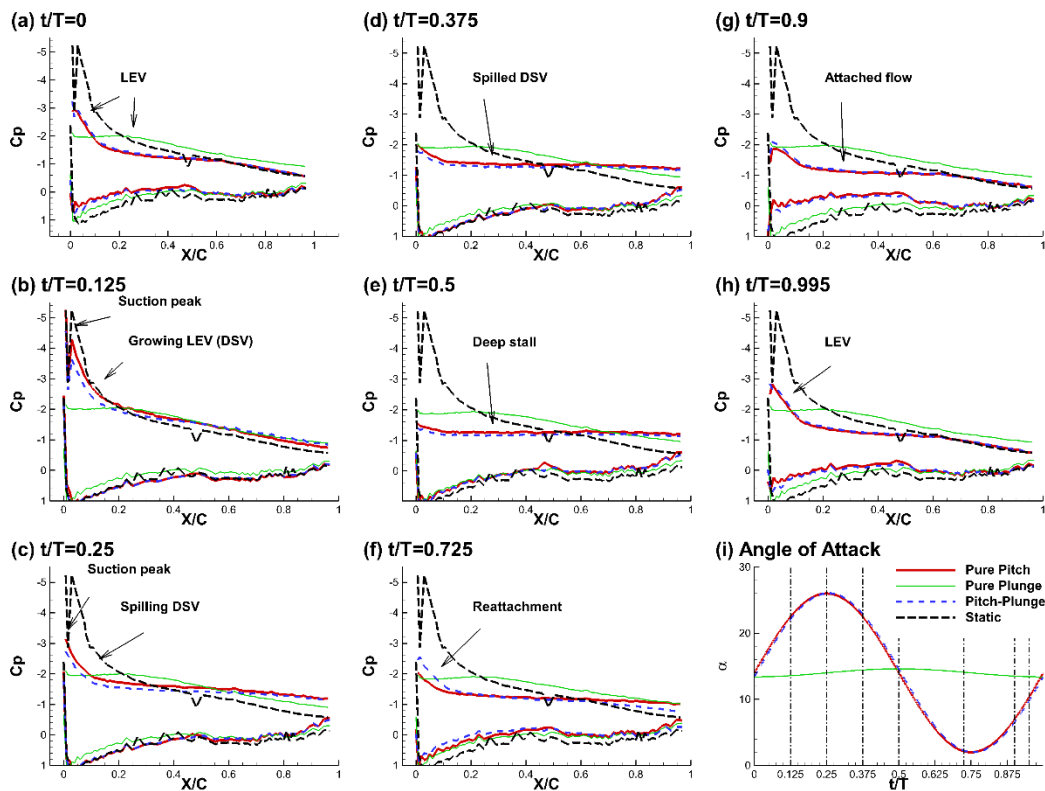


Fig. 8. Coefficient of pressure distribution for $\alpha_0=14$, $\theta_0=12$ and $h_0=60$ mm in different time intervals as shown on figures (a) to (h) and (i) is the angle of attack. Thick red solid line is pure pitching, normal green line is pure plunging and dashed blue line is combined pitch-plunge motion.

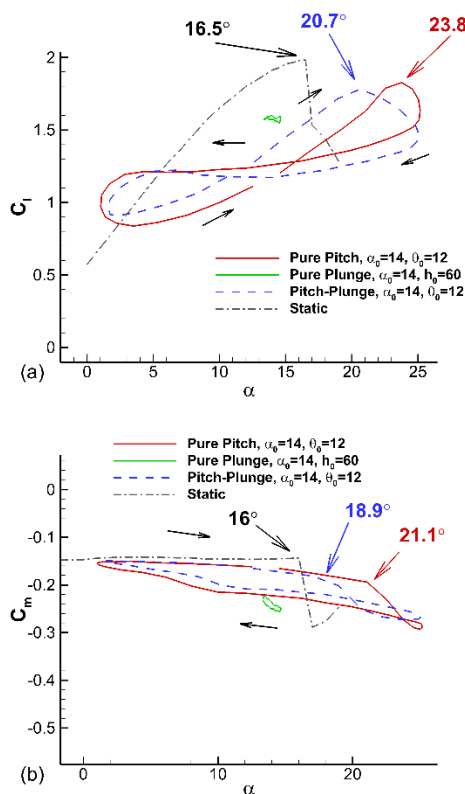


Fig. 9. (a) Lift coefficient (b) Pitching moment for $\alpha_0=14$, $\theta_0=12$ and $h_0=60$ mm.

3.4 Pitching Moment Damping Factor

Rapid drop in pitching moment and the direction of hysteresis in some specific cases can result in some structural problems such as stall flutter. Stall flutter takes place when energy is transferred from a moving airfoil to flow field during cyclic flow separation. Conversely if the moving airfoil capture the energy from the flow field the fluctuations tend to be damped and the airfoil will be stable. Also, the torsion applied to the airfoil during the oscillatory motion plays an important role in structural designs of flying objects.

To quantify the amount of torsion on the airfoil the Damping Factor (ζ) is defined as follows, in which the counter clockwise direction is assumed to be positive (Leishman (2006)). The negative values of ζ indicates unstable aeroelastic condition.

$$\zeta = -\oint C_m d\alpha \quad (6)$$

Figure 10 shows the value of Damping Factor versus mean angle of attack in pitching amplitudes of 4° and 12° . For lower amplitude of motion and before deep stall region, the direction of loops are counter clockwise and it can be interpreted that the airfoil is in a stable margin. However in $\alpha_0=14$ where the airfoil enters the deep stall condition the value of ζ is negative which shows that the airfoil is vulnerable to stall flutter. Conversely, for all cases with higher motion amplitude the value of ζ is negative, which is

a representative of instability for stall flutter. This implies that the stability of the airfoil totally depends on the amplitude of oscillation and the results show that this airfoil has the potential of stall flutter in high amplitudes. Meanwhile, applying a combined motion to the airfoil results in less negative value of ζ and it causes an increase in stability of the airfoil no matter how the amplitude of the plunge motion is small.

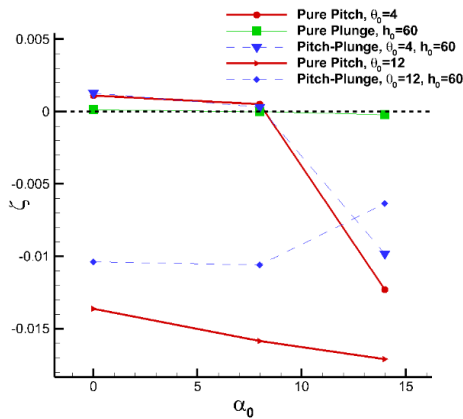


Fig. 10. Damping Factor vs. mean angle of attack.

4. CONCLUSION

The coefficients of pressure, lift and pitching moment were experimentally investigated on a supercritical airfoil which was forced to undergo pure pitching, pure plunging and combined pitching and plunging motions. Most reported results are confined to direct force measurement and surface pressure distribution has not been published as much so far, although the surface pressure provides more details of flow pattern. The experiments were performed in a closed loop wind tunnel at the Reynolds number of 8.76×10^5 and the results were collected using total number of 133 pressure tabs on the surface connected to an array of pressure transducers. We classified the results into 3 zones of pre-stall, light stall and deep stall based on the changes in the mean angle of attack. At zero mean angle of attack the LEV grew in upstroke and a little bit after and then shrunk over the upper surface while, no vortex spillage were seen over entire the motion. Also forcing the airfoil to undergo the combined motion resulted in higher phase lag in lift and pitching moment coefficients. Wherever the airfoil passed through negative angles of attack the suction peak moved to the lower surface, while for the rest of the motion the peak was located on the upper surface in low angles of attack. For all cases as the amplitude of motion increased, the combined motion got more similar to the pitching motion and it was less affected by the plunging motion. Also, most often an LSB was found over the upper surface at low positive angles of attack. In the light stall region which was represented by 8° mean angle of attack, at the starting moment of the motion the LEV grew and started to spill over the top surface of the

airfoil. Yet a tiny LEV stated near the leading edge during the stall. This mechanism occurred in deep stall region as well, but no LEV remained on the upper surface and the flow was fully separated during the stall period. Furthermore, a study was performed on the stability of the airfoil using the pitching moment Damping Factor. The results showed that for lower amplitude the airfoil is stable except for the case of deep stall, where in high amplitudes of motion it tended to enter stall flutter. Nevertheless, the combined motion improved the stability condition for all cases.

REFERENCES

- Baik, Y. S., J. Rausch, L. Bernal, & M. Ol. (2009). Experimental investigation of pitching and plunging airfoils at Reynolds number between 1×10^4 and 6×10^4 . Paper presented at the 39th AIAA fluid dynamics conference.
- Baik, Y. S., J. Rausch, L. Bernal, W. Shyy, & M. Ol. (2010). Experimental Study of governing parameters in pitching and plunging airfoil at low Reynolds number. Paper presented at the 48th AIAA aerospace sciences meeting including the new horizons forum and aerospace exposition.
- Freymuth, P. (1990). Thrust generation by an airfoil in hover modes. *Experiments in Fluids* 9 (1-2), 17-24.
- Gerontakos, P. (2004). An Experimental Investigation of Flow Over an Oscillating Airfoil. *Msc. Thesis, McGill University, Montreal, Quebec, Canada*.
- Gharali, K., and D. A. Johnson. (2014). PIV-based load investigation in dynamic stall for different reduced frequencies. *Experiments in Fluids* 55(8), 1803.
- Isogai, K., Y. Shinmoto and Y. Watanabe. (1999). Effects of dynamic stall on propulsive efficiency and thrust of flapping airfoil. *AIAA Journal* 37(10), 1145-1151.
- Jones, K. and M. Platzer. (1998). On the prediction of dynamic stall onset on airfoils in low speed flow *Unsteady Aerodynamics and Aeroelasticity of Turbomachines* (pp. 797-812): Springer.
- Kang, C. K., Y. Baik, L. Bernal, M. Ol and W. Shyy. (2009). Fluid dynamics of pitching and plunging airfoils of Reynolds number between 1×10^4 and 6×10^4 . Paper presented at the 47th AIAA Aerospace Sciences Meeting including The New Horizons Forum and Aerospace Exposition.
- Koochesfahani, M. M. (1989). Vortical patterns in the wake of an oscillating airfoil. *AIAA Journal* 27(9), 1200-1205.
- Leishman, J. G. (2006). *Principles of helicopter aerodynamics* Second Edition.
- Lian, Y., M. Ol and W. Shyy. (2008). *Comparative study of pitch-plunge airfoil aerodynamics at transitional reynolds number*. Paper presented at

- the 46th AIAA Aerospace Sciences Meeting and Exhibit.*
- Masdari, M., M. Jahanmiri, M. R. Soltani, A. Tabrizian and M. Gorji. (2017). Experimental investigation of a supercritical airfoil boundary layer in pitching motion. *Journal of Mechanical Science and Technology* 31(1), 189-196.
- Masdari, M., M. Seyednia and A. Tabrizian. (2018). An experimental loading study of a pitching wind turbine airfoil in near-and post-stall regions. *Journal of Mechanical Science and Technology* 32(8), 3699-3706.
- McAlister, K. W., L. W. Carr and W. J. McCroskey. (1978). Dynamic stall experiments on the NACA 0012 airfoil.
- McCroskey, W. (1982). Unsteady airfoils. *Annual review of fluid mechanics* 14(1), 285-311.
- McGowan, G., A. Gopalarathnam, M. Ol and J. Edwards. (2009). Analytical, computational, and experimental investigations of equivalence between pitch and plunge motions for airfoils at low Reynolds numbers. *AIAA Paper*, 535, 2009.
- Mulleners, K. and M. Raffel. (2012). The onset of dynamic stall revisited. *Experiments in Fluids* 52(3), 779-793.
- Negi, P. S., R. Vinuesa, A. Hanifi, P. Schlatter and D. S. Henningson. (2018). Unsteady aerodynamic effects in small-amplitude pitch oscillations of an airfoil. *International Journal of Heat and Fluid Flow* 71, 378-391.
- Negi, P. S., R. Vinuesa, P. Schlatter, A. Hanifi and D. S. Henningson. (2017). *Unsteady aerodynamic effects in pitching airfoils studied through large-eddy simulations*. Paper presented at the *TSFP DIGITAL LIBRARY ONLINE*.
- Radespiel, R. E., J. Windte and U. Scholz. (2007). Numerical and experimental flow analysis of moving airfoils with laminar separation bubbles. *AIAA Journal*, 45(6), 1346-1356.
- Raffel, M., J. Kompenhans and P. Wernert. (1995). Investigation of the unsteady flow velocity field above an airfoil pitching under deep dynamic stall conditions. *Experiments in Fluids* 19(2), 103-111.
- Rival, D. and C. Tropea. (2010). Characteristics of pitching and plunging airfoils under dynamic-stall conditions. *Journal of Aircraft* 47(1), 80-86.
- S. Lai, J. and M. Platzer. (1999). Jet characteristics of a plunging airfoil. *AIAA Journal* 37(12), 1529-1537.
- Sarkar, S. and K. Venkatraman. (2008). Influence of pitching angle of incidence on the dynamic stall behavior of a symmetric airfoil. *European Journal of Mechanics-B/Fluids* 27(3), 219-238.
- Theodorsen, T., W. H. Mutchler and U. S. N. A. C. f. Aeronautics. (1935). *General Theory of Aerodynamic Instability and the Mechanism of Flutter*: National Advisory Committee for Aeronautics.
- Tuncer, I. H. and M. Kaya. (2003). Thrust generation caused by flapping airfoils in a biplane configuration. *Journal of Aircraft* 40(3), 509-515.
- W.Carr, L. and T. Cebeci. (1985). *Boundary Layers on Oscilating Airfoils*.
- Young, J. and J. C. S. Lai. (2004). Oscillation frequency and amplitude effects on the wake of a plunging airfoil. *AIAA Journal* 42(10), 2042-2052.